Advection of mass fraction in forced, homogeneous, compressible turbulence

X. D. Cai, E. E. O'Brien, and F. Ladeinde
Department of Mechanical Engineering, State University of New York at Stony Brook, Stony Brook, New York 11794-2300

In nearly isothermal, compressible turbulence of a nondense gas the mass fraction of an embedded passive scalar satisfies the same formal conservation equation as a passive scalar in incompressible turbulence. Direct numerical simulation of this system shows that the compressible turbulence modes are less efficient than the incompressible in transporting scalar spectral content from large to small scales. It is argued that the cause of this outcome is the reduced size of the integral length scale of the compressible velocity components vis á vis that of the incompressible velocity components, and this also explains the experimentally observed ineffectiveness of the dilatational velocity modes in determining scalar flux in homogeneous, compressible turbulence with a uniform mean scalar gradient. © *1998 American Institute of Physics.* [S1070-6631(98)00609-6]

I. INTRODUCTION

From linearized analyses to direct numerical simulations, previous studies have demonstrated that the evolution behavior of compressible turbulence is determined by the turbulent Mach number, M_t, and the initial conditions on density, pressure and temperature fluctuations.[1–3] As a consequence of different M_t and initial conditions, compressible turbulence typically changes very rapidly at the initial stage, then arrives, asymptotically, at one of three distinct states: (a) nearly incompressible, solenoidal flow dominated by vorticity, (b) flow characterized by near statistical equilipartition of energy in vortical and compressive modes, or (c) nearly pure acoustic turbulence dominated by dilatational, compressive modes. These states are labeled, respectively, as cases S, E, and D in this article. The relative fraction of kinetic energy in acoustic modes increases from S to D and also changes the density and velocity intensity scalings with turbulent Mach number as well as the energy spectral shape.[1,4] It has also been found that the increase in compressibility in going from case S through E to D causes a change in the evolution of the Reynolds stresses.[5] There is some evidence that an increase in compressibility may have only a marginal influence on the efficiency of the turbulence in transporting and mixing of an embedded passive scalar, although this aspect has not received the attention given to the turbulence itself. In the following work we address this issue specifically in the case of nearly isothermal, compressible turbulence.

The transport equation for mass fraction, Y, of a species embedded in a flow with velocity $\mathbf{u}(\mathbf{x},t)$ can be written as

$$\frac{\partial Y}{\partial t} + \mathbf{u} \cdot \nabla Y = -\frac{1}{\rho} \nabla \cdot (\rho \mathbf{J}), \qquad (1)$$

where $\mathbf{J}$ is the scalar flux vector. From Williams,[5] if the molecular weights of the fluid and the scalar species are

equal, if gravity is the only external force, and if the thermal diffusion of the scalar is ignored, $\mathbf{J}$ can be described by Fick's law,

$$\mathbf{J} = -D \nabla Y, \qquad (2)$$

where D is the binary diffusion coefficient of the scalar in the carrier fluid. Kinetic theory of nondense gases[6] can be used to obtain an approximate expression for the diffusion coefficient, D.

$$D = 3k^0 T / (16 n m_{12} \sigma_{12} \bar{v}_{12}),$$

where k^0 is the Boltzman constant, m_{12} is the reduced mass of the binary system, n is the number of molecules per unit volume, σ_{12} is the collision cross section for molecules of types 1 and 2 and $\bar{v}_{12}$ is the average relative velocity of molecules of types 1 and 2. $\bar{v}_{12}$ is expected to be proportional to the molecular kinetic velocity which is of order $T^{1/2}$, where T is the temperature. Since n is proportional to ρ, which is of order P/T, where P is the pressure, we have the following approximate scaling relationships with temperature:

$$\rho \sim T^{-1}; \quad D \sim T^{3/2}; \quad \rho D \sim T^{1/2}.$$

This suggests that, in compressible turbulence with modest temperature fluctuations, the simplifying assumption,

$$\rho D = \text{const}, \qquad (3)$$

may be more defensible than the more common assumption of a constant diffusion coefficient.

In this study of the effect of compressibility on the transport of a scalar we have reduced the complexity of Eq. (1) by adopting both Eqs. (2) and (3) in order that only two stochastic variables D (or ρ) and $\mathbf{u}$ determine the evolution of Y. Then Eq. (1) becomes

$$\frac{\partial Y}{\partial t} + \mathbf{u} \cdot \nabla Y = D \nabla^2 Y. \qquad (4)$$

It should also be noted that, in statistically homogeneous circumstances, both Y and its Favre-averaged fluctuations, defined as $Y'' = Y - (\langle \rho Y \rangle / \langle \rho \rangle)$, satisfy Eq. (4) since both $\langle \rho Y \rangle$ and $\langle \rho \rangle$ can readily be shown to be constants in space and time. The remainder of this article will focus on the Favre fluctuation Y''. It obeys an advection diffusion equation which is formally identical to the often-studied passive scalar in incompressible turbulence, but differs from it in having both solenoidal and dilatational modes in $\mathbf{u}$, and a diffusivity which is a random variable.

In this study we extend a previous investigation[7] to consider the spectral behavior of Favre-averaged mass fraction fluctuations in three types of forced compressible turbulence, vis á vis its behavior in solenoidal turbulence. The approach is direct numerical simulation, which is outlined in Sec. III. First we derive an expression for the ratio of scalar flux due to compressible modes to scalar flux due to solenoidal modes.

II. LAGRANGIAN INTEGRAL TIME SCALES IN HOMOGENEOUS, COMPRESSIBLE TURBULENCE

We consider the motion of a fluid particle in stationary, homogeneous, compressible turbulence by adopting the Lagrangian procedure of Taylor's diffusion by continuous movements.[8]

If $\mathbf{X}(\mathbf{a},t)$ is the position at time t of a particle which was initially at $\mathbf{a}$ and $\mathbf{v}(\mathbf{a},t)$ is its velocity, then

$$X_j(\mathbf{a},t) = \mathbf{a}_j + \int_0^t v_j(\mathbf{a},\tau) d\tau.$$

Because the flow is statistically homogeneous, there exists a generalized Fourier transform of $\mathbf{v}$, say, $\widetilde{\mathbf{v}}$. Adopting Moyal's[9] decomposition of $\mathbf{v}$ in Fourier space we obtain

$$\mathbf{v}^m(\mathbf{a},t) = \int \exp(-i\mathbf{k}\cdot\mathbf{a})\widetilde{\mathbf{v}}^m(\mathbf{k},t)d\mathbf{k}, \quad m = \text{S,D},$$

$$\widetilde{\mathbf{v}}^D(\mathbf{k},t) = \mathbf{k}\frac{\mathbf{k}\cdot\widetilde{\mathbf{v}}}{|\mathbf{k}|^2}, \quad \widetilde{\mathbf{v}}^S(\mathbf{k},t) = \widetilde{\mathbf{v}}(\mathbf{k},t) - \widetilde{\mathbf{v}}^D(\mathbf{k},t),$$

where superscripts S and D are, respectively, the solenoidal and dilatational (compressible) components of the velocity,

$$\mathbf{v}(\mathbf{a},t) = \mathbf{v}^S(\mathbf{a},t) + \mathbf{v}^D(\mathbf{a},t).$$

$\widetilde{\mathbf{v}}^S(\mathbf{k},t)$ and $\widetilde{\mathbf{v}}^D(\mathbf{p},t)$ are orthogonal but so are $\mathbf{v}^S(\mathbf{a},t)$ and $\mathbf{v}^D(\mathbf{b},t)$ as the following argument shows,

$$\langle \mathbf{v}^S(\mathbf{a},t) \cdot \mathbf{v}^D(\mathbf{b},t) \rangle = \int \langle \widetilde{\mathbf{v}}^S(\mathbf{k},t) \cdot \widetilde{\mathbf{v}}^D(\mathbf{k},t) \rangle$$
$$\times \exp[-i\mathbf{k}\cdot(\mathbf{a}-\mathbf{b})]d\mathbf{k},$$

where use has been made of the property

$$\langle \widetilde{\mathbf{v}}^S(\mathbf{k},t) \cdot \widetilde{\mathbf{v}}^D(\mathbf{p},t) \rangle = \langle \widetilde{\mathbf{v}}^S(\mathbf{k},t) \cdot \widetilde{\mathbf{v}}^D(\mathbf{k},t) \rangle \delta(\mathbf{k}-\mathbf{p}).$$

But since $\widetilde{\mathbf{v}}^S(\mathbf{k},t)$ and $\widetilde{\mathbf{v}}^D(\mathbf{k},t)$ are orthogonal, we have

$$\langle \mathbf{v}^S(\mathbf{a},t) \cdot \mathbf{v}^D(\mathbf{b},t) \rangle \equiv 0. \tag{5}$$

By isotropy this result can be written, eschewing the summation convention throughout this section, as

$$\langle v_j^S(\mathbf{a},t) v_j^D(\mathbf{b},t) \rangle = 0, \quad j = 1,2,3.$$

Hence the asymptotic variance of the displacement of a fluid point can be written

$$\langle (X_j - a_j)^2 \rangle \simeq 2t(\langle (v_j^S)^2 \rangle \Lambda_{jj}^S + \langle (v_j^D)^2 \rangle \Lambda_{jj}^D),$$

where Λ_{jj}^S and Λ_{jj}^D are, respectively, the solenoidal and dilatational Lagrangian integral time scales, defined by

$$\Lambda_{jj}^m = \int_0^\infty \frac{\langle v_j^m(\mathbf{x},t) v_j^m(\mathbf{x},t+\tau) \rangle}{\langle (v_j^m)^2 \rangle} d\tau, \quad m = \text{S,D}.$$

The relative sizes of Lagrangian integral time scales can be deduced in the case of a uniform mean gradient scalar in a flow with scalar fluctuations, which are statistically homogeneous.[10] Writing scalar flux $\langle \rho v Y'' \rangle$ in the direction of increase of the mean scalar field with constant gradient β, it follows that

$$\langle \rho v Y'' \rangle = \langle \rho v^S Y'' \rangle + \langle \rho v^D Y'' \rangle$$
$$= -\beta(\langle (v_j^S)^2 \rangle \Lambda_{22}^S + \langle (v_j^D)^2 \rangle \Lambda_{22}^D).$$

Hence the ratio, r, of dilatational scalar flux to solenoidal scalar flux can be written

$$r = \frac{\langle \rho v^D Y'' \rangle}{\langle \rho v^S Y'' \rangle} = \frac{\langle (v_j^D)^2 \rangle}{\langle (v_j^S)^2 \rangle} \frac{\Lambda_{22}^D}{\Lambda_{22}^S}.$$

It is convenient to adopt the kinetic energy parameter $\chi = [\langle (v_j^D)^2 \rangle / \langle (v_j)^2 \rangle]$, which is the ratio of kinetic energy per unit mass in the dilatational modes to the total kinetic energy per unit mass, and which is the definition commonly used in the literature.[7,11] Then we find,

$$r = \frac{\chi}{1-\chi} \frac{\Lambda_{22}^D}{\Lambda_{22}^S}. \tag{6}$$

Numerical simulation of scalar flux in compressible turbulence with a uniform mean scalar gradient by Blaisdell et al.,[11] showed that r is negligibly small, even when χ is finite. Equation (6) implies that the Lagrangian integral time scale Λ_{22}^D is much smaller than the Lagrangian integral time scale, Λ_{22}^S. We will return to Eq. (6) in Sec. V, where spectral computations show that the compressible modes are less efficient than the solenoidal modes in transporting scalar intensity from low wave number to high wave number regions of the spectrum. Both these spectral and physical space transport results are explained by a shorter integral scale for the compressible modes.

III. NUMERICAL SIMULATION OF FORCED, COMPRESSIBLE HOMOGENEOUS TURBULENCE

The numerical method used in this article is based on the essentially nonoscillatory (ENO) method developed by Shu and Osher.[12] Details of its application to decaying homogeneous compressible turbulence are available in Ref. 13 and will not be repeated here. Since this study invokes transport of a passive scalar, the turbulent motion can be simulated without reference to the embedded scalar. Details of the scalar field simulations are presented in Sec. IV.

To generate approximately stationary, compressible, homogeneous turbulence fields with zero mean velocity, we have adopted the technique of Kida and Orszag[14] whereby an artificial external force at low wave number is added to the momentum and energy conservation equations. In nondimensional Eulerian form, the defining equations are

$$\frac{\partial \rho}{\partial t} + \frac{\partial}{\partial x_i}(\rho u_i) = 0, \tag{7}$$

$$\frac{\partial}{\partial t}(\rho u_i) + \frac{\partial}{\partial x_j}(\rho u_i u_j) = -\frac{\partial p}{\partial x_i} + \frac{\partial}{\partial x_j}(d_{ij}) + \rho F_i, \tag{8}$$

$$\frac{\partial}{\partial l}(\rho e_T) + \frac{\partial}{\partial x_j}[(\rho e_T + p)u_j]$$

$$= \frac{\partial}{\partial x_i}\left(d_{ij}u_j + \frac{\mu}{(\gamma-1)P_r}\frac{\partial T}{\partial x_i}\right) + \rho u_i F_i, \tag{9}$$

where e_T is the nondimensional total energy given by $e_T = e + \frac{1}{2}u_j u_j$, e is the nondimensional internal energy, $d_{ij} = \mu[(\partial u_i/\partial x_j)+(\partial u_j/\partial x_i)-(2/3)(\partial u_k/\partial x_k)\delta_{ij}]$ is the deviatoric stress tensor and the second coefficient of viscosity, μ_2, is taken as $\mu_2 = -\frac{2}{3}\mu$. As done by Cai et al.,[15] the velocity scale is chosen to be u_0^*, the speed of sound divided by the square root of the ratios of specific heats, that is, $u_0^* = (R^*T_0^*)$, where R^* is the specific gas constant and T_0^* is the initial mean temperature. Since the mean flow field in homogeneous turbulence has no intrinsic length scale, we choose an arbitrary length scale, L_0^*, as the reference length, and the time scale is L_0^*/u_0^*. The density is scaled by the initial mean density, ρ_0^*, so that $\rho = \rho^*/\rho_0^*$. For consistency, the temperature, T, pressure, p, and energy per unit mass are nondimensionalized by, respectively, the initial mean temperature, T_0^*, the initial mean pressure, p_0^*, where $p_0^* = \rho_0^* R^* T_0^*$, and the mean square velocity $|u_0^*|^2$. The viscosity is nondimensionalized as $\mu = 1/Re_0 = \mu^*/\rho_0^* u_0^* L_0^*$, μ^* is assumed constant and Re_0 is the reference Reynolds number. The Prandtl number, $P_r = \mu^* C_p^*/\sigma^*$, where σ^* is the thermal conductivity and C_p^* is the specific heat, is also constant. In all the above definitions the superscript (*) denotes a dimensional variable. The artificial external force, F_i, has the form

$$F_i(\mathbf{x},t) = A_{ij}(t)\sin(x_j) + B_{ij}(t)\cos(x_j),$$

where $\mathbf{A}(t) = \{A_{ij}(t)\}$ and $\mathbf{B}(t) = \{B_{ij}(t)\}$ are Gaussian random variables with zero means. Each element of $\mathbf{A}(t)$ and $\mathbf{B}(t)$ is assumed to be statistically independent. The diagonal and off-diagonal parts of $\mathbf{A}(t)$ and $\mathbf{B}(t)$ represent, respectively, the compressive and noncompressive parts of $\mathbf{F}$, or, in other words, the longitudinal and transverse excitations. In the present simulations, the second-order moments of the diagonal and off-diagonal elements are chosen to satisfy

$$\langle A_{ij}^2(t)\rangle = \langle B_{ij}^2(t)\rangle = \begin{cases} \dfrac{2F_c}{3\Delta t}, & \text{if } i=j, \\[2ex] \dfrac{F_R}{3\Delta t}, & \text{if } i\neq j, \end{cases}$$

TABLE I. Forcing scheme and flow parameters.

Case	S	E	D
Δt	0.02	0.02	0.01
$\dfrac{1}{3\Delta t}F_R$	$\sqrt{1/34}$	$\dfrac{1}{7}$	0
$\dfrac{2}{3\Delta t}F_c$	0	$\sqrt{1/5}$	$\sqrt{3/4}$
q_t	0.0972	0.113	0.113
M_t	0.340	0.371	0.404
λ	1.244	1.186	1.148
R_λ	53.5	58.3	58.4
η	0.0860	0.0792	0.0779
χ	0.0111	0.587	0.990
I_ρ	0.0498	0.259	0.359

where Δt is the time step, whose value and those of F_c and F_R can be found in the first three rows of Table I, where the Reynolds number $Re_0 = 200$. As noted by Cai et al.,[15] under the condition of the low Reynolds number $Re_0 = 200$ with 64^3 mesh, the ENO scheme can resolve the spectrum in the wave number range $k \leq 20$, which includes the energetic modes of principal interest in the study of advection. A 64^3 mesh is adopted in these three-dimensional (3D) simulations of spectral evolution from initial scalar spectra in which intensity is concentrated in low wave number modes.

Through the use of this scheme we have successfully produced three distinct types of approximately stationary, homogeneous, compressible turbulence which are labeled in Table I as solenoidal, S, equipartition, E, and dilatational, D. The identifying letter indicates the relative energy content in the solenoidal and dilatational modes. For example, E indicates approximate equipartition in energy between the two modal types. S and D denote, respectively, almost entirely solenoidal and almost entirely dilatational modes.

In the remaining rows of Table I, the obtained values of important flow parameters, averaged over the computational temporal-spatial domain, are presented for each of the three types of turbulence. They are defined as follows: total kinetic energy, $q_t = \frac{1}{2}\langle u_i u_i\rangle$; turbulent Mach number, $M_t = u_{\text{rms}}/c$; Taylor microscale, $\lambda = (\epsilon/5\mu u_{\text{rms}}^2)^{-1/2}$; Taylor microscale Reynolds number, $R_\lambda = (5/3\mu\epsilon)^{1/2}\langle\rho\rangle\langle u_i u_i\rangle$; Kolmogorov length scale, $\eta = [(\mu^3/\epsilon)^{1/4}/\langle\rho\rangle^{1/2}]$; ratio of kinetic energy in compressible modes to total kinetic energy, $\chi = \langle u_i^D u_i^D\rangle/\langle u_i u_i\rangle$; density relative intensity, $I_\rho = \rho'_{\text{rms}}/\langle\rho\rangle$. In this definition $\epsilon = \mu[4/3\langle(\partial u_i/\partial x_i)^2\rangle + \langle\omega^2\rangle]$, $u_{\text{rms}} = \langle u_i u_i\rangle^{1/2}$, and c is the average sound speed: $c = \langle(\gamma RT)^{1/2}\rangle$.

The parameters in Table I have been purposely chosen to produce the three types of turbulence S, E and D, in order to display a wide diversity in kinetic energy ratio, χ, which by definition satisfies $0 \leq \chi \leq 1$. Simultaneously, they display approximately equal values of total kinetic energy, q_t, turbulent Mach number, M_t, and Reynolds number, R_λ. An increase in the ratio of energy content in compressible modes, χ, corresponds to an increase in the relative intensity of density fluctuations, I_ρ.

The purpose of generating a compressible turbulence which is approximately statistically stationary is to simplify

and clarify the role of compressibility in transporting an embedded passive scalar. Since transport by all scales of compressible turbulence, large and small, is expected to be significant, the dynamics of a decaying turbulence would unavoidably complicate the kinematics of scalar evolution, except, perhaps, if, at large Reynolds number, a statistically stationary regime of the turbulence were to develop at very small scales, and we were interested only in the scalar properties at those scales. We have neither the high Reynolds number computational capability nor an interest confined to the small scales of the scalar field. Therefore we have attempted to produce stationary, compressible turbulence induced by a driving force at the largest scales, and we examine the spectral evolution of the scalar from distributions which initially have intensity predominantly in the low wave number regime. The nature of the driving force will clearly play a role in the details of scalar spectral evolution. As we show in Sec. IV, there is a stark difference between the computed results for the evolution of the scalar spectrum by solenoidal velocity modes and those by dilatational modes, results large enough to justify, we believe, some general conclusions about the role of compressibility in passive scalar transport. An alternative approach would be to generate random compressible velocity fields, independent of the equations of motion, by manipulation of random number generation, but that appears to be even less closely related to Navier–Stokes homogeneous turbulence, itself a somewhat artificial construct.

While it is desirable to obtain a statistically stationary, turbulent velocity, it is impossible to judge precisely if a time series is statistically stationary unless it is known over large (technically, infinite) periods. It is also impossible to know definitely when an initially evolving quantity becomes statistically stationary. Thus, the judgment of stationarity is somewhat subjective and uncertain. The concerns about this uncertainty of judgment depend on how seriously the results depend on the stationarity. In our case, studies are focused on a qualitative assessment of the compressibility effects on scalar transport due to various compressible turbulent fields with decidedly different kinetic energy ratios, but without rapidly changing velocity statistics. For our purpose a looser, more subjective judgment suffices to indicate approximately statistical stationarity.

Figure 1 shows the simulation results for the evolution of kinetic energy in the S, E, and D cases. As the flow field is excited by the random force at the largest scales, kinetic energy grows from an initially zero value until it reaches a stable mean value (listed in Table I), when the smallest-scale motions reach statistical equilibrium under the effects of advection and viscous dissipation. The oscillatory phenomena shown in Fig. 1 are a consequence of the Gaussian random force introduced at the largest scales.[14] Figures 2, 3, and 4 show the evolutions of another two important parameters, the Kolmogorov length scale (η) and the Taylor length scale (λ), for each type of turbulence. In contrast to the strong oscillatory behavior observed in the evolution of kinetic energy, the oscillations of the Kolmogorov length scale are much smaller due to the strong smoothing effects of molecular viscosity. Loosely speaking, statistical quasiequilibrium is
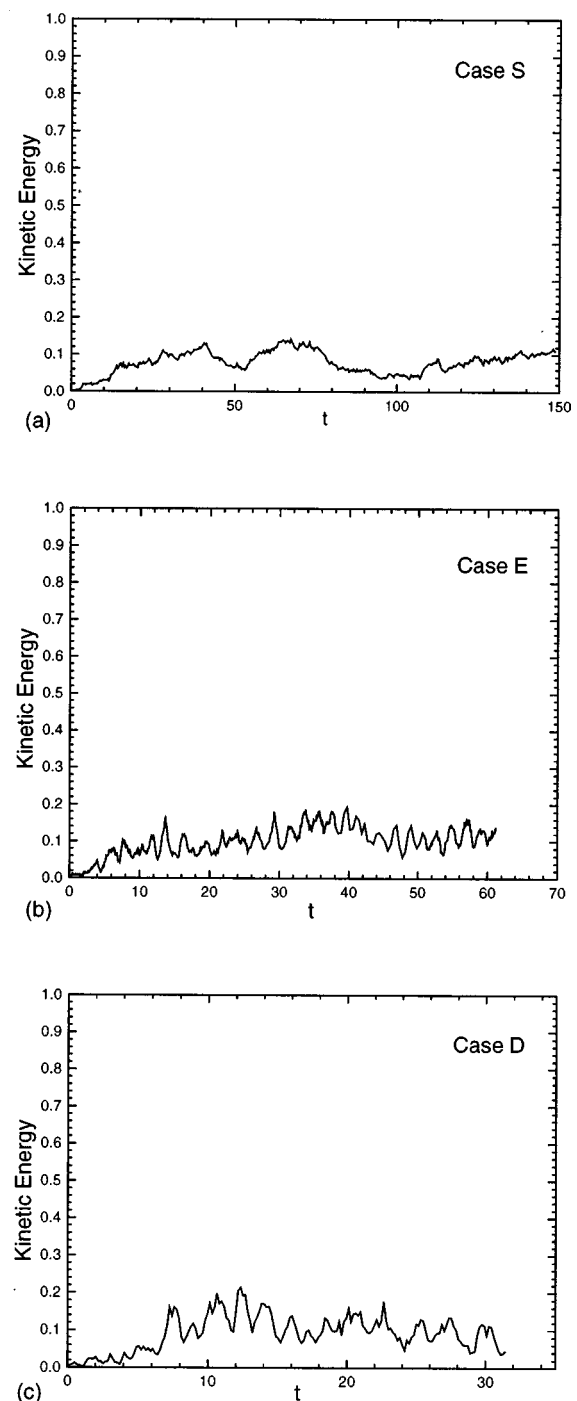

FIG. 1. Evolution of kinetic energy in cases (a) S, (b) E, and (c) D.

observed for the S case after $t \simeq 110$, for the E case after $t \simeq 40$, and for the D case after $t \simeq 15$. In a quasiequilibrium state, the statistical quantities of small scale, such as the dissipation rate and Kolmogorov length scale, are relatively smooth with variance smaller than 1% while large scale statistical quantities, such as q_t, M_t, and R_λ (not shown) show quasiperiodic behaviors with variances around 10%. Figure 5 shows the spectral distribution of compressible and solenoidal energy in the quasistationary state for each of the three types of turbulence. In order to simulate a passive scalar embedded in each of the three types of compressible turbulence, the scalar field is turned on at a point when the veloc-
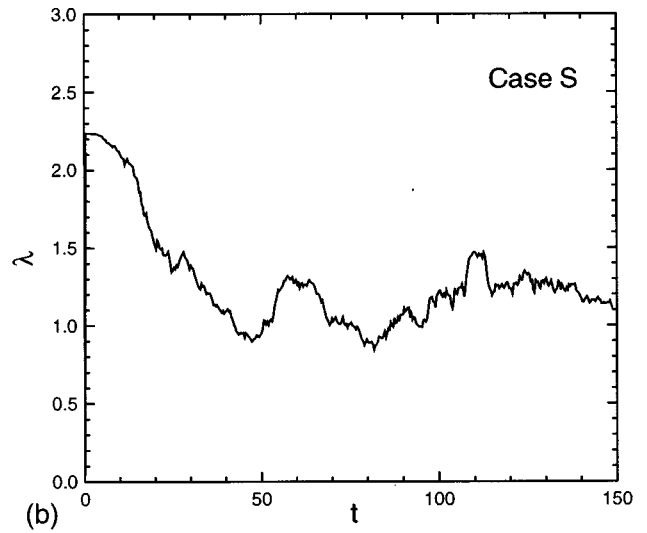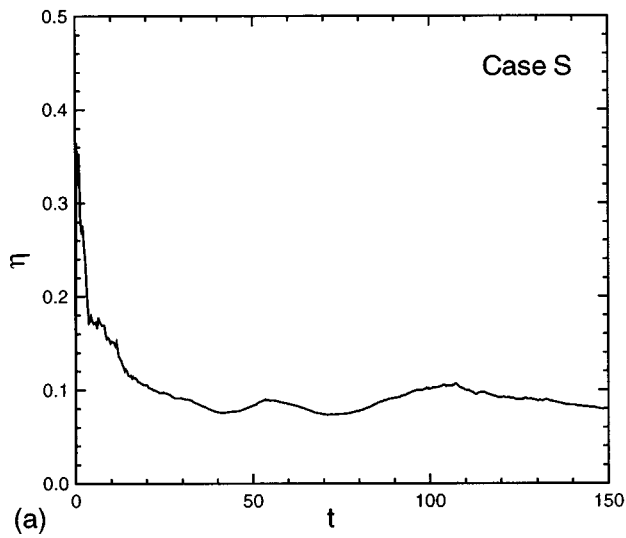
FIG. 2. Evolution of characteristic parameters in case S: (a) Kolmogorov length scale (η) and (b) Taylor length scale (λ).
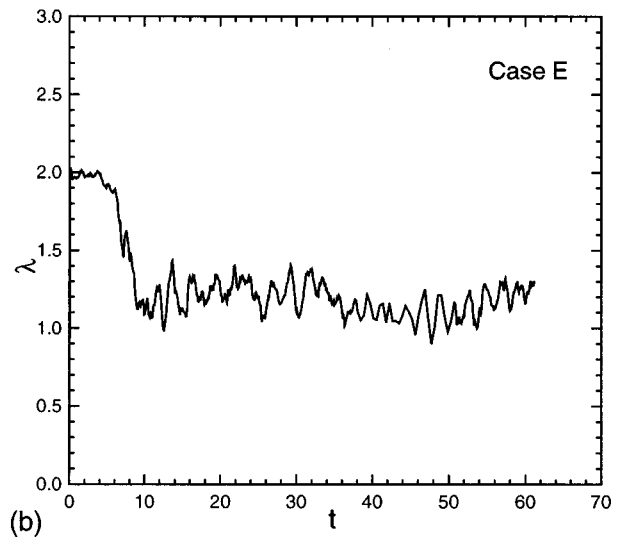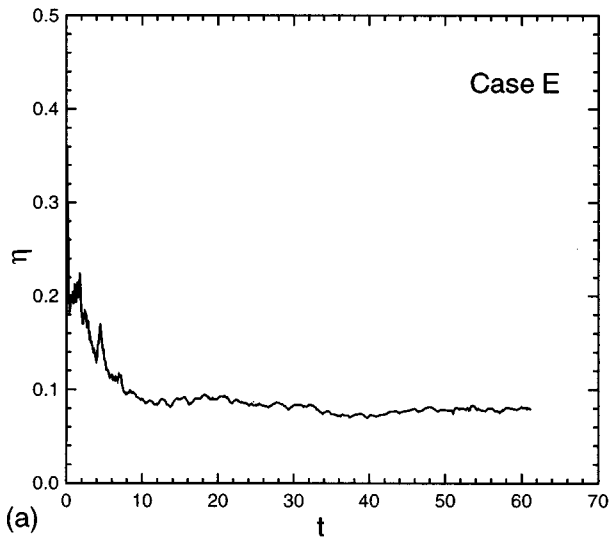

FIG. 3. Evolution of characteristic parameters in case E: (a) Kolmogorov length scale (η) and (b) Taylor length scale (λ).
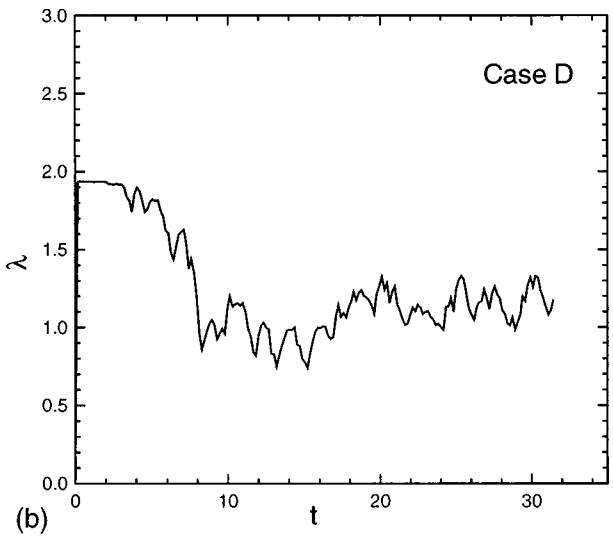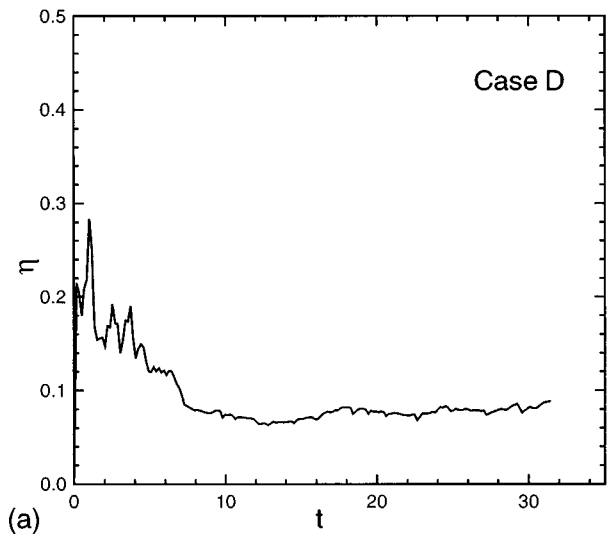

FIG. 4. Evolution of characteristic parameters in case D: (a) Kolmogorov length scale (η) and (b) Taylor length scale (λ).
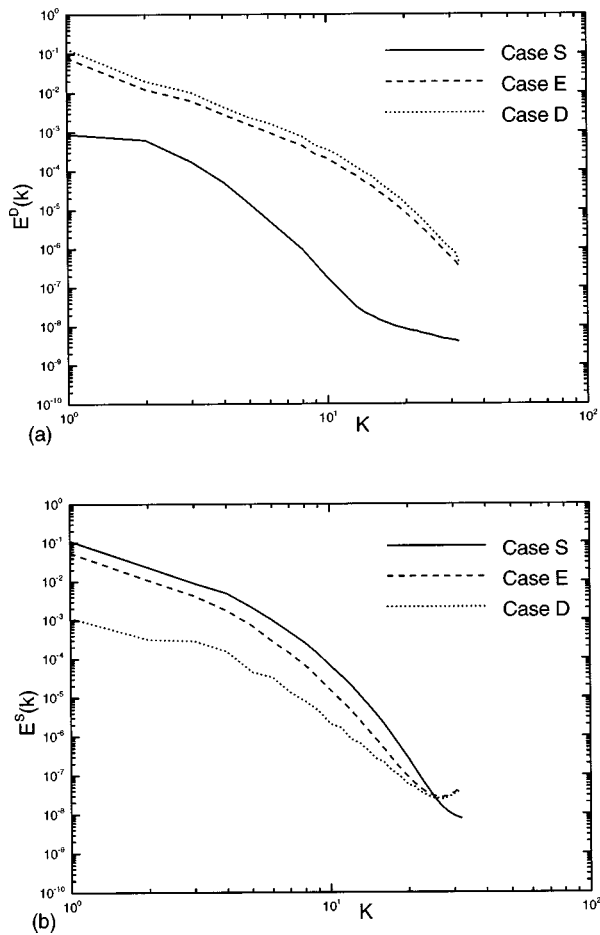
FIG. 5. Time-averaged stationary kinetic energy spectra: (a) dilatational energy spectra, $E^D(k)$ and (b) solenoidal energy spectra, $E^S(k)$.

ity field is quasistationary, and starts from $t = 131.9$–139.5 for the S case, from $t = 50.8$–61.2 for the E case, and from $t = 16.9$–24.4 for the D case. The flow parameter values in Table I are temporal-spatial averages starting from the initiation of the scalar field at these times.

IV. NUMERICAL SIMULATION OF THE PASSIVE SCALAR

Initial conditions for scalar $Y''(\mathbf{x},0)$ are generated from a random variable $\psi(\mathbf{k},0)$, in Fourier space, of the form

$$\psi(\mathbf{k},0) = E_{Y''}(k,0) \exp[2\pi i \theta(\mathbf{k})],$$

where $\theta(\mathbf{k})$ is a uniformly distributed random number between 0 and 1, $k = \|\mathbf{k}\|$, and $E_{Y''}(k,0)$ is a prescribed term. To ensure that $Y''(\mathbf{x}, 0)$ is real when transformed to the physical space, we set

$$\psi(-\mathbf{k},0) = \psi^*(\mathbf{k},0),$$

where ψ^* is the complex conjugate of ψ. Finally, we transform $\psi(\mathbf{k},0)$ into physical space and normalize all nodal values of Y'' by their root mean square (rms) value.

To generate a scalar field with specific initial properties, a more refined method can be used to modify the above procedure. For example, to generate a scalar field with double-delta probability distribution, three steps are taken.[16]

TABLE II. Initial integral scales.

Case	S/S1	E/S1	D/S1	S/S2	E/S2	D/S2
$(l)_0$	2.04	1.94	1.71	2.04	1.94	1.71
$(l_{Y''})_0$	0.426	0.426	0.426	0.741	0.741	0.741
$\left(\dfrac{l_{Y''}}{l}\right)_0$	0.209	0.220	0.249	0.363	0.382	0.433

(a) First, the above procedure is used to generate a random scalar field in Fourier space.

(b) Next, the scalar field is transformed into physical space. In physical space, the scalar value at each node is reset to 1 if it is positive, and to -1 if it is negative. This operation yields the desired double-delta distribution but also causes the scalar value to change abruptly between adjacent nodes, thereby producing significant high-wave number components in the scalar field, which are poorly resolved in the simulations.

(c) Finally, the scalar field is retransformed into Fourier space. The Fourier amplitudes of the scalar are multiplied by a filter function, $F(k)$, defined by

$$F(k) = \begin{cases} 1 & k \leq k_c \\ (k/k_c) & k > k_c \end{cases}$$

where k_c is a specified cutoff wave number. This filtering operation removes many of the poorly resolved high-wave number components of the scalar fields.

Two distinct initial scalar spectra have been used in this study. The initial scalar spectrum for the first case, labeled S1, is

$$E_{Y''}(k,0) \sim \begin{cases} \exp[-0.1(k_x^2 + k_y^2 + k_z^2)] & k \leq 3.0, \\ 0 & k > 3.0, \end{cases}$$

and, for the second case, S2,

$$E_{Y''}(k,0) \sim \begin{cases} \dfrac{1}{k^2} & k \leq 1. \\ 0 & k > 1. \end{cases}$$

The treatment of random numbers is different in the two cases. In the S1 case numbers are generated by the first procedure described above, while S2 numbers are generated using the second procedure in which the cutoff wave number, k_c, in the filter function is 2. Because of this difference in their generation procedure S1 and S2 have different initial probability distributions. S1 has a near-Gaussian distribution and S2 has almost a double-delta distribution.

There is evidence from numerical simulations of incompressible turbulence that scalar evolution is less sensitive to the initial spectral shape of the scalar[17] than to the ratio of initial integral length scales of the scalar and the turbulence.[16] Thus, it is anticipated that there will be differences in the subsequent evolutions of the scalar spectra in cases S1 and S2, especially at small times, and these will mostly be due to the differences in the initial scalar/velocity integral length scale ratios.

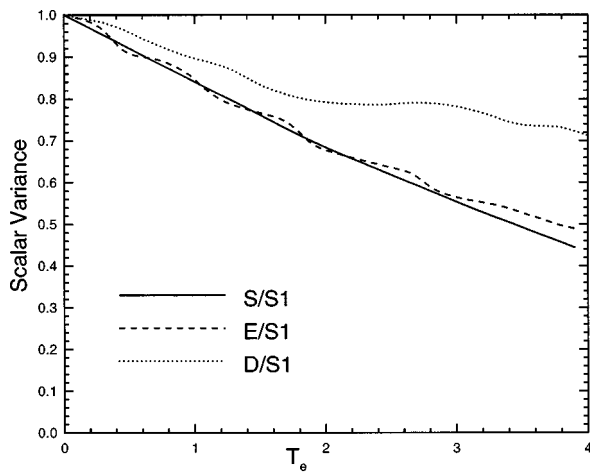In Table II, the initial length scales of the scalar and the

FIG. 6. Evolution of scalar variance in S/S1, E/S1, and D/S1 cases. T_e is eddy-turnover time.

velocity, and their ratios, are given for each type of turbulence S, E, and D and for both types of initial scalar spectra, S1 and S2.

The initial velocity integral length scale, $(l)_0$, is defined by

$$(l)_0 = \frac{3\pi}{4} \frac{\int_0^\infty k^{-1} E^S(k,0)dk}{\int_0^\infty E^S(k,0)dk},$$

where $E^S(k,t)$ is the energy spectrum of the solenoidal modes of the turbulence, and $(l_{Y''})_0$ the scalar integral length scale is given by

$$(l_{Y''})_0 = \frac{\pi \int_0^\infty k^{-1} E_{Y''}(k,0)dk}{4 \int_0^\infty E_{Y''}(k,0)dk},$$

where $E_{Y''}(k,t)$ is the spectrum of scalar intensity.

In the definition of $(l)_0$, the initial energy spectrum of the incompressible modes, $E^S(k,0)$, is preferred to the total energy spectrum $E(k,0)$, because it is in incompressible turbulence that the phenomenon of the effect of integral length scale ratio on scalar evolution was established,[16] and the constant $3\pi/4$ with definition of $(l)_0$ is obtained for solenoidal flows. However, if $E^S(k,0)$ is replaced by $E(k,0)$, the values of $(l)_0$ in Table II are altered by less than 10%. Furthermore, as the results in Sec. V will show, the integral length scale for the compressible velocity modes is much smaller than the integral length scale of the solenoidal modes and is, therefore, likely to be less effective in determining the behavior of scalar evolution.[16]

V. SCALAR FIELD SIMULATION RESULTS

The evolution of scalar variance is presented in Fig. 6 for the S1 cases of scalar transport (the time unit used here and later on is the eddy-turnover time based on Taylor scale, λ/u_{rms}). The initial scalar spectrum for these cases is provided in Fig. 7(a), and has scalar intensity compacted in the large scales. It can be seen from Fig. 6 that the decay rate of scalar variance in the S/S1 case differs sharply from the decay rate in the D/S1 case, which, we speculate, is a consequence of a difference in the nature of the interaction of the

solenoidal and dilatational velocity modes with the scalar fluctuations. Dilatational modes are dominant in the D/S1 case, which suggests that the much slower decrease of scalar variance in this case is due to a slower spectral transport to the more dissipative higher wave numbers by the dilatational modes. Simultaneously the S/S1 case shows the most rapid decrease in scalar variance, or, equivalently, the most rapid spectral transport of scalar intensity to the smaller scales. On the other hand, the distinction between results for the S/S1 and E/S1 cases is very small. However, we note that the E/S1 case has a solenoidal energy spectrum similar to that of the S/S1 case, although the dilatational spectra differ sharply (see Fig. 5). If the dilatational modes are less effective in scalar spectral transport than the solenoidal modes, this would also explain the S/S1 and E/S1 results. The same behavior of the scalar variances has been reproduced in the S2 cases[18] (not shown).

This interpretation is also supported by simulations of scalar variance spectral evolution in cases S/S1, E/S1 and D/S1 (Fig. 7), which begin with the same initial scalar variance spectrum but with distinctly different velocity fields (see Fig. 5). In all of the S1 cases it can be seen that the high-wave number scalar variations begin from states of negligible energy and, in general, after one eddy-turnover time, appear approximately steady as a consequence of turbulent distortion and an increase of scalar gradient which take place much more quickly than the overall decay of the scalar field.[15] At the same time, the phenomenon of higher spectral intensity levels in the S/S1 case than in the D/S1 case at high wave numbers (larger than $k=4$ in this case), and the reverse at the smallest wave numbers, implies a faster spectral transfer in S/S1 than in D/S1. The same behavior of scalar variance spectra has also been observed for the S/S2, E/S2, and D/S2 cases (Fig. 8). It is noted that all the S2 cases have the same initial scalar variance spectrum, which differs significantly from that of the S1 cases. Returning to Fig. 5, it can be seen that, even though the total kinetic energy is almost the same, the incompressible energy spectra, $E^S(k)$, and compressible energy spectra, $E^D(k)$, are at quite different levels, except for the solenoidal spectra, $E^S(k)$, of S and E type turbulence, and the dilatational spectra, $E^D(k)$, of E and D type turbulence. The dilatational strain rate, $[k^3 E^S(k)]^{1/2}$, dominates in D cases while the solenoidal strain rate, $[k^3 E^S(k)]^{1/2}$, dominates in S cases. This difference in the mode of velocity strain rate gives rise to a difference in the development of the scalar variance spectra (Figs. 7 and 8). In Fig. 9 the spectra of scalar gradient for both S1 and S2 cases are displayed. They also show a similar behavior whereby the D cases appear to be less efficient than the S cases in developing the small scale structure of the mass fraction field.

It is worthwhile here to examine directly the advective effects of dilatational and solenoidal velocity modes on scalar gradient. As illustrated in the work of Corrsin,[19] Obukhoff,[20] and Batchelor,[21] the development of the scalar variance spectrum is determined by the action of the turbulent motion on the scalar distribution by introducing a continual reduction of the length scale of scalar variations. During this process, the random convection of material elements
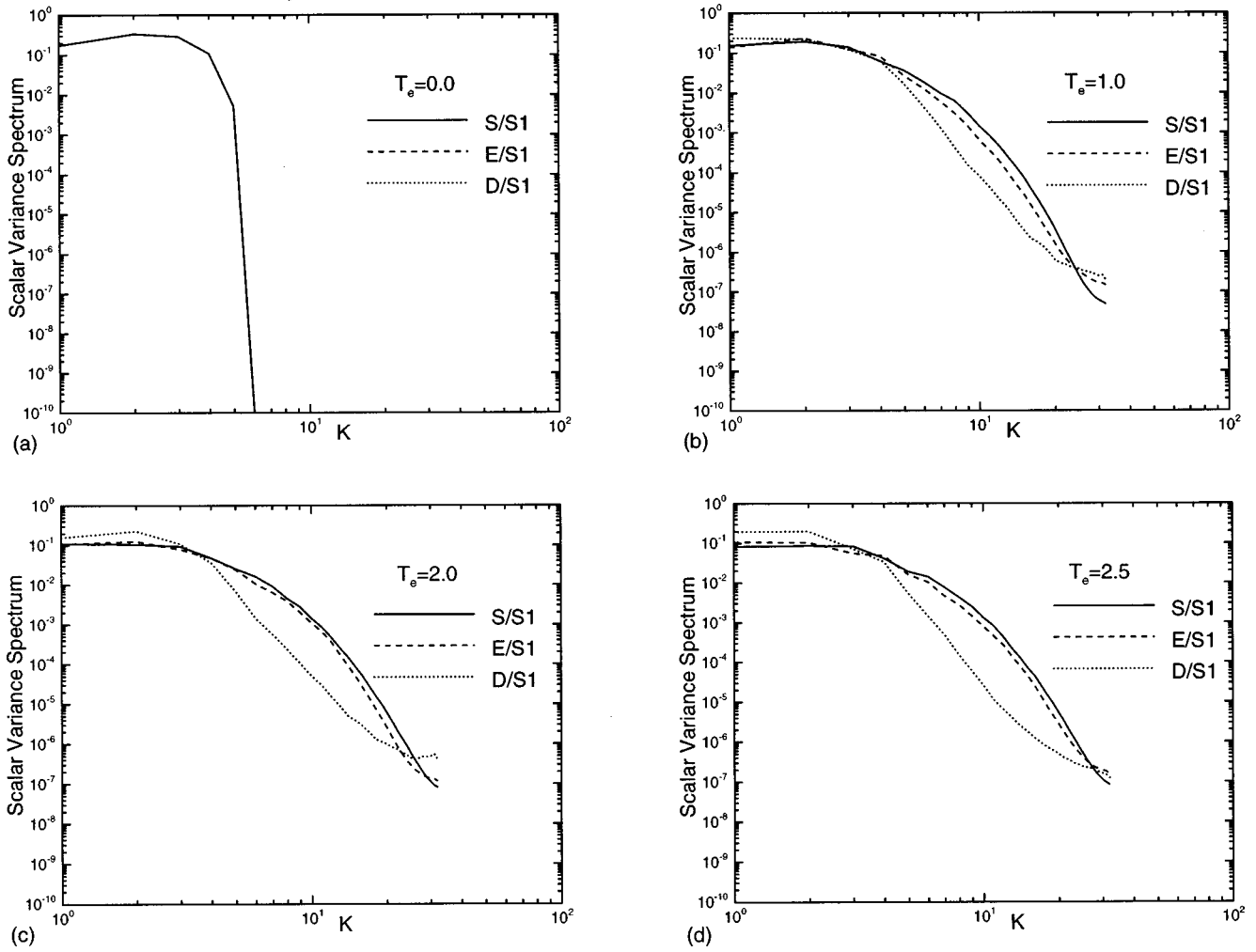
FIG. 7. Development of scalar variance spectra in S1 cases: (a) $T_e=0$, (b) $T_e=1.0$, (c) $T_e=2.0$, and (d) $T_e=2.5$. T_e is eddy-turnover time.

of the fluid is inevitably accompanied by distortion of these elements and an (statistical) increase in the gradients of the scalar in the absence of molecular conduction. This mechanism can be illustrated by a simple rapid distortion analysis of the development of scalar gradient in a compressible flow.

Using Eq. (4), we obtain the following equation for scalar gradient:

$$\frac{d}{dt}\left(\frac{\partial Y''}{\partial x_i}\right) = -\frac{\partial u_j}{\partial x_i}\frac{\partial Y''}{\partial x_j} + D\frac{\partial^2}{\partial x_k \partial x_k}\left(\frac{\partial Y''}{\partial x_i}\right)$$
$$+ \frac{\partial D}{\partial x_k}\frac{\partial^2 Y''}{\partial x_k \partial x_k}.$$

If the molecular diffusion terms are ignored, the mean square scalar gradient satisfies

$$\frac{d}{dt}\left(\frac{\partial Y''}{\partial x_i}\right)^2 = -2\frac{\partial u_j}{\partial x_i}\frac{\partial Y''}{\partial x_j}\frac{\partial Y''}{\partial x_i},$$

where the summation convention is not used. That is, $i=1,2,$ or 3.

In a principal axis reference frame, with the following simplified strain rate assumptions,

$$\frac{\partial u_1^l}{\partial x_1} = s(t) = -\frac{\partial u_2^l}{\partial x_2}, \quad \frac{\partial v_3^l}{\partial x_3} = 0,$$

$$\frac{\partial u_1^C}{\partial x_1} = \frac{\partial u_2^C}{\partial x_2} = \frac{\partial u_3^C}{\partial x_3} = \frac{1}{3}d(t),$$

$$\frac{\partial u_i^l}{\partial x_j} \equiv 0, \quad i \neq j,$$

we find

$$\frac{d}{dt}\left(\frac{\partial Y''}{\partial x_1}\right)^2 = 2\left(-s - \frac{1}{3}d\right)\left(\frac{\partial Y''}{\partial x_1}\right)^2,$$

$$\frac{d}{dt}\left(\frac{\partial Y''}{\partial x_2}\right)^2 = 2\left(s - \frac{1}{3}d\right)\left(\frac{\partial Y''}{\partial x_2}\right)^2,$$

$$\frac{d}{dt}\left(\frac{\partial Y''}{\partial x_3}\right)^2 = -\frac{2}{3}d\left(\frac{\partial Y''}{\partial x_3}\right)^2.$$

On integrating these equations one finds,

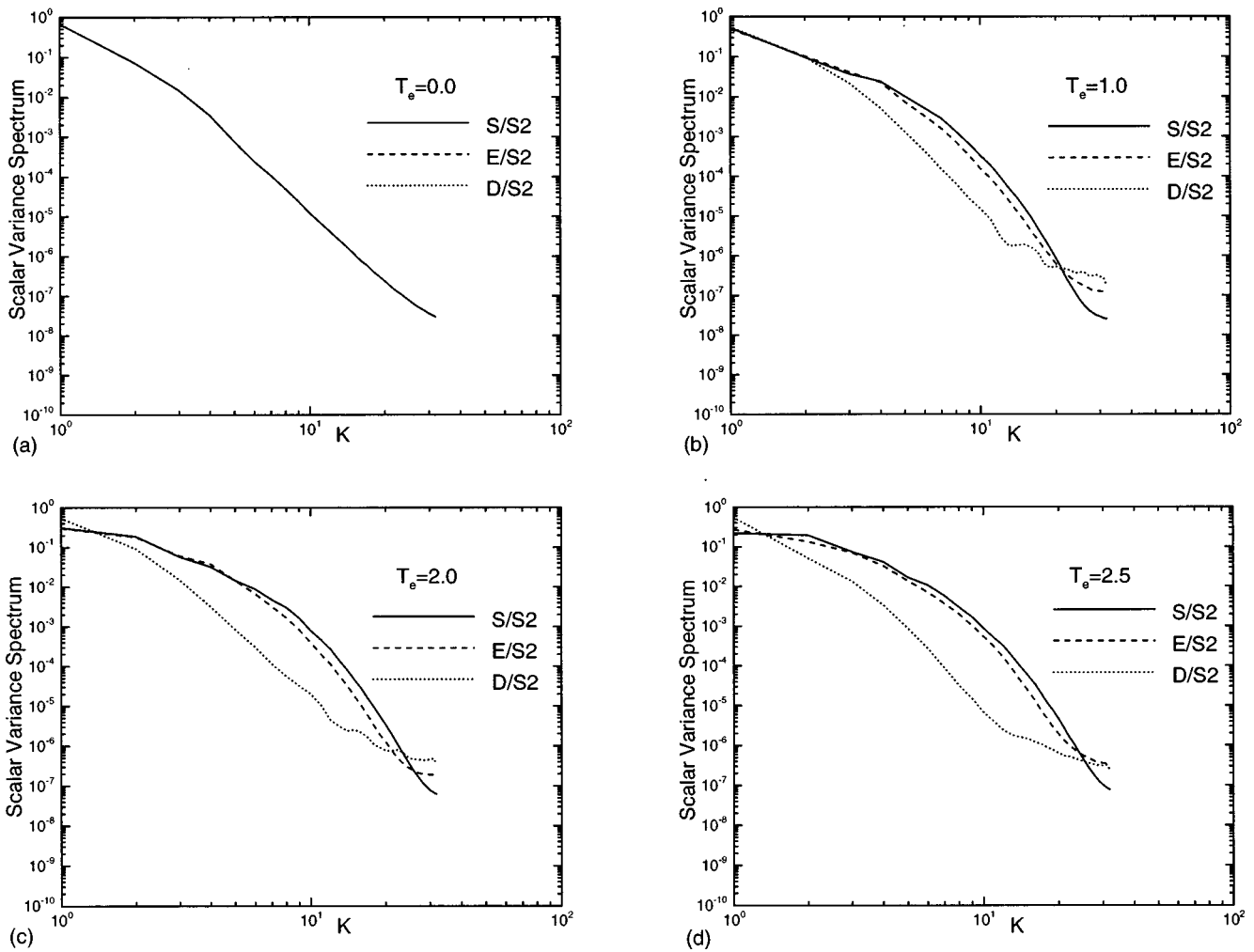FIG. 8. Development of scalar variance spectra in S2 cases: (a) $T_e = 0$, (b) $T_e = 1.0$, (c) $T_e = 2.0$, (d) $T_e = 2.5$. T_e is eddy-turnover time.

$$(\nabla Y'')^2 = (\nabla Y'')_0^2 \left(2\cosh \int_0^t 2s(\tau)d\tau + 1 \right)$$

$$\times \exp\left(-\frac{2}{3}\int_0^t d(\tau)d\tau \right), \tag{10}$$

where $(\nabla Y'')_0^2$ is the initial value of $(\nabla Y'')^2$.

Clearly the dissipation rate of the scalar, $\epsilon_{Y''}$, is affected differently by the irrotational strain rate $s(t)$ and the dilatational strain rate $d(t)$, although both play a role in its evolution. In particular, while the sign of $d(t)$ in Eq. (10) is relevant, the sign of $s(t)$ is not. From the analysis of Sarkar et al.,[22] $d(t)$ is expected to have a pseudoperiodic behavior similar to that of the dilatational velocity $\mathbf{u}^D$, and its time scale to be of the order of the integral time scale of the compressible velocity, and, therefore, to be much shorter than the corresponding integral time scale of the solenoidal velocity, as implied by Eq. (6) which will be revisited in the next paragraph. In such a case, $d(t)$ oscillates rapidly compared to rates of change of $s(t)$ and, therefore, the exponential term in Eq. (10), which is dependent on $d(t)$, is expected to be less effective in developing $(\nabla Y'')^2$ than $s(t)$ is. There is no claim here that dilatational strain rate has a negligible effects on scalar dissipation, merely that the solenoidal ve-

locity component is more efficient in the production of scalar gradient by the velocity field stretching mechanisms. The numerical results, displayed in Figs. 6–8 for the evolution of scalar variance and its spectra, and in Fig. 9 for the evolution of scalar gradient spectra, are consistent with this simple rapid distortion model. Figure 10 shows the variance of scalar gradient in the S1 cases as a function of time. The asymptotic crossover of the D/S1 case is easily traced to the slower decrease of scalar gradient intensity in the low wave number regions of the spectra presented in Fig. 9.

We return now to Eq. (6) and the ineffectiveness of dilatational modes in transporting a scalar in physical space, which was observed by Blaisdell et al.[11] in a numerical study of scalar flux with a uniform mean scalar gradient in homogeneous, compressible turbulence. They showed that the contribution from dilatational velocity to the scalar flux term is small compared to the contribution from solenoidal velocity, even when the fraction of kinetic energy in the compressible mode, χ, is large. From Eq. (6), and noting that our expression for scalar flux $\langle \rho v Y'' \rangle$ in this simple configuration is equal to theirs, it can be concluded that their observation implies that the Lagrangian integral time scale of the solenoidal velocity must be larger than that of the dilatational
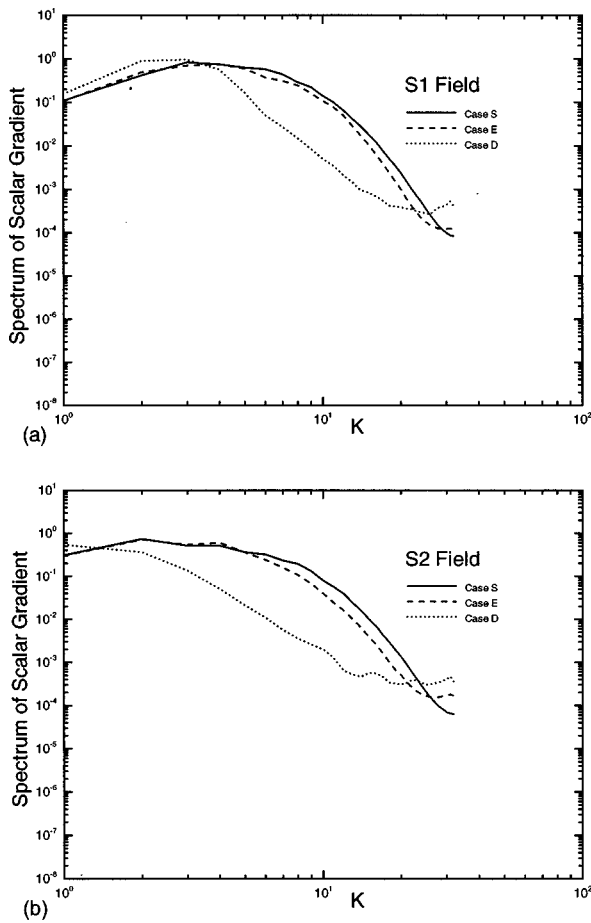
FIG. 9. Spectra of scalar gradients at $T_e = 2.0$: (a) S1 cases and (b) S2 cases.

FIG. 11. Eulerian velocity correlation in case E: $(- - -)$ solenoidal velocity correlation and $(—)$ dilatational velocity correlation.

velocity. From our simulation of case E, a time-averaged ratio of Lagrangian integral time scale of dilatational velocity to solenoidal velocity is estimated to be 0.079, according to Eq. (6), if a sliding-averaged scalar flux calculation is used.

In Fig. 11 we display the spatial distribution of the Eulerian velocity correlation in the E case for both the solenoidal and dilatational modes. The Eulerian integral length scale
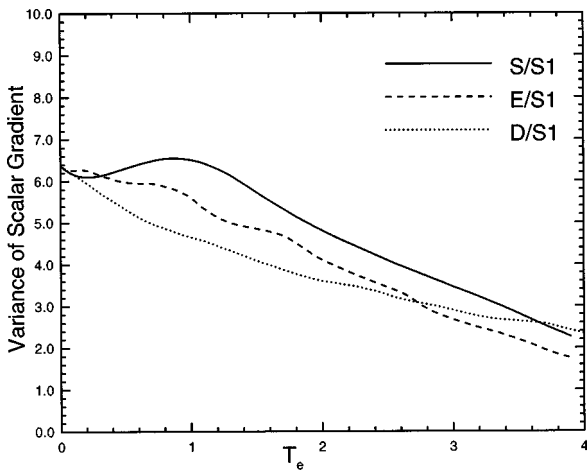

FIG. 10. Evolution of mean square scalar gradient, $\langle (\partial Y''/\partial x_i)(\partial Y''/\partial x_i) \rangle$, in S/S1, E/S1, and D/S1 cases. T_e is eddy-turnover time.
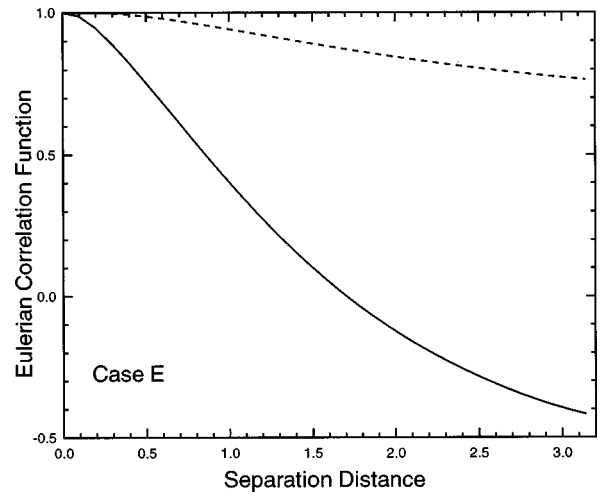
is clearly much larger for the solenoidal modes. The time scales of Eq. (6) can be connected to the more accessible Eulerian length scale by assuming an approximate equality of Lagrangian and Eulerian velocity time correlations in low Reynolds number flow, as suggested by Burgers and proposed by Corrsin.[23] That is,

$$\langle v_j^m[\mathbf{X}(\mathbf{a},t),t]v_j^m[\mathbf{X}(\mathbf{a},t),t+\tau]\rangle$$

$$\approx \langle u_j^m(\mathbf{x},t)u_j^m(\mathbf{x},t+\tau)\rangle, \quad m = S,D.$$

In a homogeneous, compressible flow confined in a box,[24] $\langle v_j^2 \rangle = \langle u_j^2 \rangle$. If an additional assumption, such as Taylor's approximation of frozen flow, is used with $\langle u_0 \rangle = \sqrt{(\rho_0/\rho_0)}$, the Eulerian velocity spatial correlation can determine the Lagrangian integral time scale. Since Fig. 11 clearly shows that the Eulerian integral length scale of dilatational velocity is much smaller than the solenoidal velocity integral length scale in the E case, and similar behavior is observed in all computed cases, the explanation for the relative weak scalar transport by dilatational modes, observed by Blaisdell et al.,[11] lies with the small value of their Lagrangian integral time scale.

VI. CONCLUSIONS

Three-dimensional simulations of a dynamically passive mass fraction, transported by three cases of homogeneous, compressible turbulence, each with distinctly different levels of compressible energy content, have been carried out in this 3D numerical study. In situations of small temperature fluctuation the mixture fraction obeys the classic passive scalar advection-diffusion equation, except that the velocity field has both dilatational and solenoidal modes and the diffusivity is a random variable. The focus of this work is on the advective effects of the dilatational modes, which are shown to be much less effective than the solenoidal modes in transporting the scalar field variance content from large scale to small scale regions of its spectrum. The cause is traced to a large discrepancy between the sizes of the respective integral length scale for the dilatational and solenoidal modes. An

idealized rapid distortion analysis supports the notion that dilatational modes are less effective in scalar spectral transport than the solenoidal modes. Computations have shown that the dilatational modes contribute little to the scalar flux in compressible turbulence with a uniform mean scalar gradient.[11] This result is consistent with the smallness of the integral length scale of dilatational velocity components. It is also consistent with recent studies on the effects of compressibility on Reynolds stress,[25–27] wherein the reduction of the integral length scale by compressibility plays a key role. It is a part of a model which captures the steep decrease in the growth rate of fully developed free-shear layers as the convective Mach number increases.

A similar phenomenon must also occur with advective transport of other scalar quantities such as partial density, ρY, or concentration. In these cases the role of density is more complex. In particular, a direct effect of velocity dilatation on scalar evolution is added to advection by solenoidal and dilatational modes, as can be seen if the mass conservation equation for density is combined with Eq. (1).

ACKNOWLEDGMENT

[1] S. Ghosh and W. H. Matthaeus, ''Low Mach number two-dimensional hydrodynamic turbulence: Energy budgets and density fluctuations in a polytropic fluid,'' Phys. Fluids A **4**, 148 (1992).

[2] G. P. Zank and W. H. Matthaeus, ''The equations of nearly incompressible fluids. I: Hydrodynamics, turbulence, and waves,'' Phys. Fluids A **3**, 69 (1991).

[3] T. Passot and A. Pouquet, ''Numerical simulation of compressible homogeneous flows in the turbulent regime,'' J. Fluid Mech. **181**, 441 (1991).

[4] S. K. Lele, ''Compressibility effects on turbulence,'' Annu. Rev. Fluid Mech. **26**, 211 (1991).

[5] F. A. Williams, *Combustion Theory*, 2nd ed. (Benjamin–Cummings, Menlo Park, CA, 1985).

[6] J. O. Hirschfelder, C. F. Curtiss, and R. B. Bird, *Molecular Theory of Gases and Liquids* (Wiley, New York, 1954).

[7] F. Ladeinde, E. E. O'Brien, X. D. Cai, and W. Liu, ''Advection by polytropic compressible turbulence,'' Phys. Fluids **7**, 2843 (1995).

[8] G. I. Taylor, ''Diffusion by continuous movements,'' Proc. London Math. Soc. **20**, 196 (1921).

[9] J. E. Moyal, ''The spectra of turbulence in a compressible fluid: Eddy turbulence and random noise,'' Proc. Cambridge Philos. Soc. **48**, 329 (1951).

[10] S. Corrsin, ''Heat transfer in isotropic turbulence,'' J. Appl. Phys. **23**, 113 (1952).

[11] G. A. Blaisdell, N. N. Mansour, and W. C. Reynolds, ''Compressibility effects on the passive scalar flux within homogeneous turbulence,'' Phys. Fluids **6**, 3498 (1994).

[12] C.-W. Shu and S. Osher, ''Efficient implementation of essentially nonoscillatory shock-capturing schemes,'' Comput. Phys. **77**, 439 (1988).

[13] F. Ladeinde, E. E. O'Brien, and X. D. Cai, ''A parallelized ENO procedure for direct numerical simulation of compressible turbulence,'' J. Sci. Comput. **11**, 179 (1996).

[14] S. Kida and S. A. Orszag, ''Energy and Spectral Dynamics in Forced Compressible Turbulence,'' J. Sci. Comput. **5**, 85 (1990).

[15] X. D. Cai, E. E. O'Brien, and F. Ladeinde, ''Thermodynamic behavior in decaying compressible turbulence with initially dominant temperature fluctuations,'' Phys. Fluids **9**, 1754 (1997).

[16] V. Eswaran and S. B. Pope, ''Direct numerical simulations of the turbulent mixing of a passive scalar,'' Phys. Fluids **31**, 506 (1988).

[17] V. Eswaran and E. E. O'Brien, ''Simulations of scalar mixing in grid turbulence using an eddy-damped closure model,'' Phys. Fluids A **1**, 537 (1989).

[18] X. D. Cai, ''Compressible turbulence and its transport of a passive scalar,'' Ph.D. dissertation, State University of New York at Stony Brook, 1997.

[19] A. M. Obukhoff, ''Structure of the temperature field in turbulent flows,'' Izv. Akad. Nauk SSSR, Geogr. Geophys. Ser. **13**, 58 (1949).

[20] S. Corrsin, ''On the spectrum of isotropic temperature fluctuations in isotropic turbulence,'' J. Appl. Phys. **22**, 469 (1951).

[21] G. K. Batchelor, ''Small scale variation of convected quantities like temperature in a turbulent fluid, part I,'' J. Fluid Mech. **5**, 113 (1959).

[22] S. Sarkar, G. E. Erlebacher, M. Y. Hussaini, and H. O. Kreiss, ''The analysis and modeling of dilatational terms in compressible turbulence,'' J. Fluid Mech. **227**, 473 (1991).

[23] S. Corrsin, in *Mecanique de la Turbulence*, edited by A. Favre (CNRS, Paris, 1962).

[24] H. Tennekes and J. L. Lumley, *A First Course in Turbulence* MIT Press, Cambridge, 1972.

[25] S. Sarkar, ''The stabilizing effect of compressibility in turbulent shear flow,'' J. Fluid Mech. **282**, 163 (1995).

[26] A. W. Vreman, N. D. Sandham, and K. H. Luo, ''Compressible turbulent mixing layer growth rate and turbulence statistics,'' J. Fluid Mech. **320**, 235 (1996).

[27] A. Yoshizawa, W. W. Liou, N. Yokoi, and T.-H. Shih, ''Modeling of compressible effects on the Reynolds stress using a Markovianized two-scale method,'' Phys. Fluids **9**, 3024 (1997).